IEEE Access
Multidisciplinary | Rapid Review | Open Access Journal

Received August 26, 2020, accepted September 14, 2020, date of publication September 18, 2020,
date of current version September 30, 2020.

Digital Object Identifier 10.1109/ACCESS.2020.3025005

Performance Analysis of Optical-CDMA for Uplink Transmission in Medical Extra-WBANs

MD JAHID HASAN[1,2], MOHAMMAD ALI KHALIGHI[1], (Senior Member, IEEE), JORGE GARCÍA-MÁRQUEZ[3], AND BASTIEN BÉCHADERGUE[2]

[1]Aix-Marseille University, CNRS, Centrale Marseille, Institut Fresnel, Marseille, France
[2]Oledcomm SAS, 78140 Vélizy-Villacoublay, France
[3]Pôle Photonique-Energétique, Laboratoire National de Métrologie et d'Essais, 78190 Trappes, France

Corresponding author: Mohammad Ali Khalighi (ali.khalighi@fresnel.fr)

This work was supported by the European Union's Horizon 2020 research and innovation programme under the Marie Skłodowska-Curie grant agreement No. 764461 (VisIoN).

ABSTRACT This paper considers the use of infrared wireless communications for uplink transmission in extra wireless body-area networks. We focus on a multi-user medical application, where the collected medical data of several patients inside a hospital room is transmitted to one or several access points (APs). For this uplink transmission, we investigate the performance of optical code-division multiple access in asynchronous mode, while taking into account the effect of random transmitter orientation. For this purpose and to consider realistic scenarios, we implement an orientation-based random waypoint mobility model to consider the mobility of patients inside a hospital ward. Performance evaluation is done in terms of the link average bit-error-rate and outage probability. We further investigate the performance improvement by using several APs, compared with the case of a single AP.

INDEX TERMS Wireless body area networks, medical WBAN, telemedicine, wireless optical communications, infrared data transmission, optical code-division multiple access, random waypoint model, binary pulse-position modulation.

I. INTRODUCTION

Real-time continuous monitoring of patients is crucial in hospitals or health-care centers to detect any deterioration in the patients' health conditions and to prevent inappropriate treatments. On the other hand, telemonitoring post-operative patients or elderly people at home is a very efficient way of improving the quality of life and, at the same time, reducing health-care expenditures. Such e-health solutions can be realized, in particular, through the use of wireless body-area networks (WBANs) by sending timely data from a number of on-body or implanted medical sensors [1]. Here, from a data transmission point of view, the communication architecture can be divided into intra-WBAN and extra-WBAN, where the former concerns the communication between the sensors and a central coordinator node (or hub) [2], and the latter refers to the communication between the coordinator node (CN) and an external network or an access point (AP) [3]–[5].

Recently, the use of optical wireless communications (OWC) based on visible-light (VL) and infrared (IR) links has gained increasing attention in medical WBAN applications, mainly because of their immunity against electromagnetic interference (EMI) and their license-free and inherent security features, as compared to radio-frequency (RF) links [6]. Indeed, the already-proposed RF-based solutions rely on transmission in the unlicensed ISM (Industrial, Scientific and Medical) band, which is increasingly subject to EMI. In addition, they are highly vulnerable to data interception and hacking [4].

A. UPLINK SIGNAL TRANSMISSION

In this paper, we consider the use of IR links for the case of an extra-WBAN medical network by focusing on uplink communication between a CN, placed on a patient body, and an AP. Note that we exclude the use of VL that could irritate the patient's vision. Here, special attention should be devoted to eye-safety, link reliability, and power consumption of the transceiver modules. According to the IEC-62471 (International Electro-technical Commission) standard, for pulsed IR, a cornea exposure irradiance limit of 100 W/m^2 and a retina exposure radiance limit of 545.5 $mW/mm^2/sr$ have no eye hazard at a distance of 200 mm [7]. Also, from a

The associate editor coordinating the review of this manuscript and approving it for publication was Matti Hämäläinen.

communication theory perspective, an important issue is to handle the multiple-access interference (MAI) requirement when several transmitters (i.e., CNs) have to share the same communication channel.

B. MANAGING MULTIPLE ACCESS

As a matter of fact, in typical situations, several patients may share a hospital ward, and similarly, a few elderly people may need to be monitored at a senior's residence room. Then, simultaneous data transmission from multiple patients is unavoidable, which requires the use of appropriate multiple-access (MA) techniques. Time- and code-division MA (TDMA and CDMA) are potential techniques of relatively low implementation complexity within this context. In the context of OWC-based WBANs, different variants of TDMA techniques including time-hopping, and periodic- and priority-based data transmission were proposed for multiple-patient monitoring [8]–[10]. However, these solutions do not support asynchronous data transmission from different patients. Recently, the use of optical camera communication was considered for multiple-patient monitoring inside a hospital ward [11] but this system loses its reliability in the absence of line-of-sight (LOS) links. A bandwidth-efficient sparse code MA technique was also proposed in [12] based on VL LOS links at the cost of a relatively high implementation complexity, compared to CDMA. In order to increase the robustness of the network and relax the synchronization requirement between multiple transmitters (which is obviously crucial in the case of TDMA [13]), we propose here to use the optical CDMA (O-CDMA) technique.

Data transmission is then performed using intensity modulation with direct detection (IM/DD) [14]. In this work, we consider the binary pulse-position modulation (BPPM) scheme [15]. We will later justify this choice regarding implementation simplicity.

The performance of O-CDMA depends on the signature codes used to map the data of different users [16]. The very well-known optical orthogonal codes (OOC), initially introduced for optical fiber communications [16], can be adopted here. However, in the OWC context, O-CDMA can suffer from MAI and the so-called near-far problem [17], [18] when used in asynchronous mode. In addition, patients' mobility and random transmitters (Txs) orientations may severely degrade the system performance [19], [20].

It is worth mentioning that IR OWC links can also be used for intra-WBAN data transmission. To avoid interference between intra- and extra-WBAN links, different wavelengths can be used together with optical filters at the Rxs. Therefore, reasonably, we do not consider any potential MAI corresponding to intra-WBAN connections in this paper.

C. STATE-OF-THE-ART ON OCDMA FOR OWC

The performance of O-CDMA was experimentally investigated for indoor optical wireless local-area networks in [21], [22]. The authors in [23] and [24] considered the impact of ambient noise on the diffuse IR O-CDMA channel. Also, the near-far problem and MAI effect on a diffuse IR uplink were studied in [25], [26]. In [27], O-CDMA was proposed for uplink transmission in medical extra-WBAN applications, where the effect of patients' mobility inside a hospital room was studied as well, while assuming a half-tracked LOS link between a medical sensor and an AP. Such a half-tracked link is, however, complex to implement as it requires a fine knowledge of the user and AP positions to align the Tx with the receiver (Rx). On the other hand, for intra-WBAN medical applications, the analytical study of a diffuse O-CDMA link was presented in [28], [29] based on a hard-limiter (HL) Rx structure. In a recent work, we investigated the practical implementation of O-CDMA for extra-WBAN uplink data transmission [30].

D. PROPOSED STUDY AND CONTRIBUTIONS

In this work, we study the performance of O-CDMA when used for extra-WBAN links. In contrast to the work presented in [27], we take into account the Tx power constraint due to eye-safety considerations, the different noise sources at the Rx, as well as randomly changing Tx orientations. Based on the random waypoint (RWP) model [31], [32], we further consider the user mobility in our study by using the generalized model of orientation-based RWP (ORWP) [33] in order to include the effect of random Tx orientations. Moreover, we investigate the improvement of the link quality through the use of multiple APs in the room. Performance evaluation is mainly done in terms of the link outage probability P_{out}, which is studied for the first time within this context, to the best of our knowledge.

The main contributions of this work can be summarized as follows:

- Studying the O-CDMA performance using accurate and realistic channel modeling;
- Elucidating the limitation of the O-CDMA performance in mobility conditions due to the near-far problem;
- Quantifying the link performance degradation due to LOS blockage with the presence or absence of MAI, and showing the contribution of the diffuse link;
- Demonstrating the substantial improvement in the link performance and reliability by using multiple APs.

The remainder of this paper is organized as follows. In Section II, we describe the O-CDMA system based on OOC codes as signature sequences. Next, Section III presents the mathematical formulations for studying the link performance. Numerical results are then presented in Section IV to investigate the bit-error-rate (BER) and P_{out} performances of the system for changing users' locations in the room and different AP arrangements. The main conclusions of this work and some future directions are provided in Section V.

Notations : Bold-face upper-case letters are used for matrices and lower-case letters for vectors. Also, XYZ is the reference Cartesian coordinate system, $(.)^T$ denotes transposition, $E\{.\}$ stands for expected value and $\ln(.)$ is the natural logarithm.

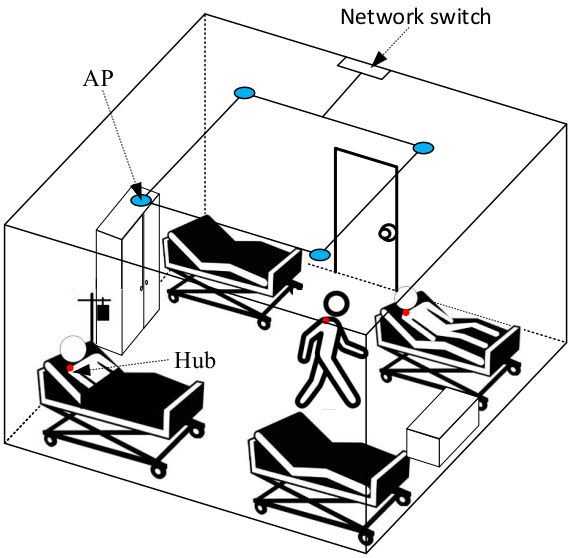

FIGURE 1. Illustration of a typical hospital ward scenario using an IR based extra-WBAN with multiple patients, each one having a CN (the red bullet on the shoulder). Here, 4 APs are considered, placed on the ceiling.

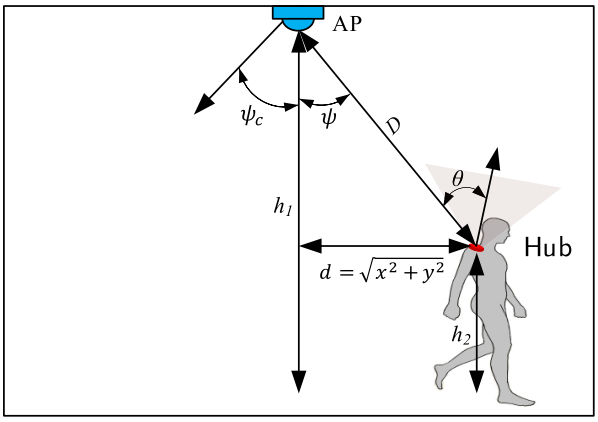

FIGURE 2. Illustration of a typical LOS link configuration between a CN and the AP. x and y represent the coordinates of the hub with respect to the room center, i.e., the AP position.

II. SYSTEM DESCRIPTION

A. GENERAL ASSUMPTIONS

Figure 1 illustrates a typical hospital ward with potentially up to four patients inside, where IR links are used for extra-WBAN uplink transmission. Note that, most hospital guidelines recommend a maximum of four patients in a ward [34].

We consider the use of IR light-emitting diodes (LEDs) because of their relatively low cost and more tolerable eye-safety features (due to the typically much wider beams), compared to laser diodes (LDs). In practice, each CN could be equipped with an IR LED, like [35], with a wavelength of 940 nm, a transmitting area of 1 mm^2 and a radiant intensity of 300 mW/sr corresponding to a typical transmit power of 1150 mW. Then, according to [7], up to 10 LEDs can be used simultaneously in this configuration and with a 50% duty cycle while still meeting the IEC "no risk group" requirements. Note that, while a typical IR LED can offer a bandwidth of about 20 MHz [35], an LD can alternatively be used for applications demanding higher data rates. In such a case, an optical diffuser should be inserted in front of the LD to break its spatial coherence and to satisfy the eye-safety requirement. However, the resulting Tx would be more expensive and bulkier, compared to the case of using an LED. Note that considering the power consumption of a battery-powered CN, we restrict the optical transmit power of an IR LED to a maximum of 280 mW.

The Tx (i.e., the CN) is considered to be placed on the shoulder of each patient, which has been shown in [36] to be an appropriate choice due to the patient comfort and also the relatively high probability of having a LOS connection with the AP(s), placed on the ceiling. Unless otherwise specified, only one single AP, placed at the center of the room ceiling, is assumed in the sequel. The AP is connected through a backbone cable to a local network switch as shown in Fig. 1. Patients are considered to be equipped with different medical sensors to monitor their temperature, blood-saturation, blood pressure, etc. (not shown in the figure). The CN collects the data from all sensors before sending them to the AP(s). The requirement in terms of data-rate for most sensors is less than 100 Kbps [37], [38]. Consequently, we consider a data-rate of up to 100 Kbps for the extra-WBAN link.

We consider a hospital ward with room dimensions $8 \times 8 \times 3\,m^3$, which satisfies the general health-care guidelines [34]. We assume a relatively large field-of-view (FOV) at the AP (with no concentrator) and the use of a simple PIN photo-detector (PD). Note that, compared with an avalanche PD (APD), the use of a PIN PD allows a less expensive and a less bulky Tx with simpler electronics, and furthermore less sensitivity to background illuminations. We denote by d the horizontal distance of the Tx from the AP, placed at the center of the room ceiling, see Fig. 2. In the figure, h_1 and h_2 are the heights of the AP and the CN, respectively.

Given the relatively low data-rate transmission, the on-off-keying (OOK) modulation would be a suitable choice due to its simplicity. Here, instead, we consider the BPPM modulation, which has almost the same performance as OOK but with the advantage that no adaptive thresholding is needed for optimal signal detection at the Rx [39], [40]. Note that, although non-binary PPM would be more advantageous in terms of energy efficiency [41], we suggest using BPPM which has the advantages of a lower required bandwidth, less constraints in terms of eye-safety, and lower implementation complexity.

B. CHANNEL MODEL

Denoting the transmit optical power by P_t and the channel attenuation or channel DC gain for the LOS link by $H_{\rm LOS}$, the received power from the LOS is given by $P_{r0} = H_{\rm LOS} P_t$. From Fig. 2, considering the Lambertian source model for the

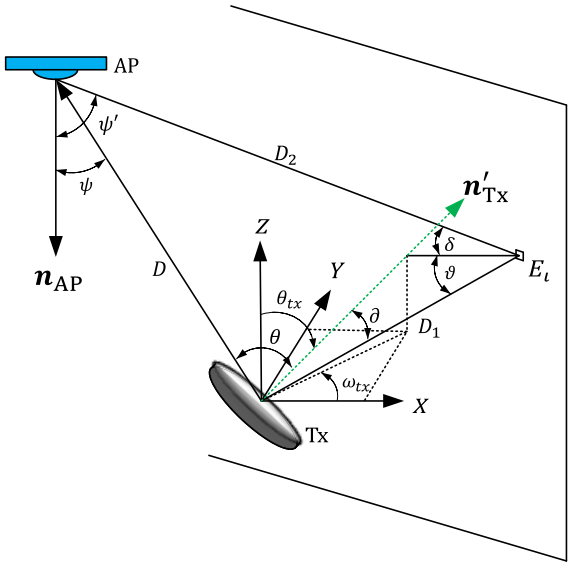

FIGURE 3. LOS and diffuse link with randomly oriented Tx. Here, θ_{tx} denotes the elevation angle, ω_{tx} is the azimuth angle, and n_{AP} and n'_{Tx} stand for the normal vectors corresponding to the AP and Rx, respectively.

LED at the Tx, we have [14]:

$$H_{\mathrm{LOS}} = \begin{cases} \dfrac{A_d(m+1)}{2\pi D^2}\cos^m(\theta)\cos(\psi) & ;\ 0 \le \psi \le \psi_c \\ 0 & ;\ \psi > \psi_c, \end{cases} \tag{1}$$

where ψ denotes the beam incident angle at the Rx, A_d is the PD's area, and θ is the radiance angle of the Tx that depends on the elevation angle θ_{tx} as shown in Fig. 3. The LOS link distance between the CN and the AP is given by $D = \sqrt{d^2 + (h_1 - h_2)^2}$. Also, ψ_c in (1) is the FOV of the Rx and m is the Lambertian order of the LED, related to its semi-angle at half power $\phi_{1/2}$ [42]:

$$m = \frac{-\ln 2}{\ln(\cos\phi_{1/2})}. \tag{2}$$

Concerning the diffuse link, we denote by H_{ref} the channel DC gain component corresponding to the signals collected from the beam reflections at the Rx. To avoid too timely simulations, here only 1$^{\mathrm{st}}$-order reflections are taken into account. Note that this choice is practically rational as most non-LOS contributions correspond to the first-order reflections [43]. To calculate H_{ref}, we consider a set of small Lambertian reflecting surface elements, each one with area A_E and reflectivity coefficient ρ, as shown in Fig. 3. For each element E_ι, the corresponding channel DC gain is given by [14], [44]:

$$H_{\mathrm{ref},\iota} = \begin{cases} \dfrac{(m+1)\rho A_d A_E}{2\pi D_1^2 D_2^2}\cos^m(\partial)\cos(\vartheta)\cos(\delta)\cos(\psi') & ;\ 0 \le \psi' \le \psi_c \\ 0 & ;\ \psi' > \psi_c, \end{cases} \tag{3}$$

where D_1 denotes the distance between the Tx and the reflecting surface element E_ι, D_2 is the distance between E_ι and the Rx, ∂ is the radiance angle of the Tx, ϑ expresses the incident angle on E_ι, δ is the radiance angle of the reflected rays from E_ι, and ψ' denotes the incident angle at the Rx (see Fig. 3).

Now the total received power P_r taking into account both LOS and the diffuse links is given by [42]:

$$P_r = \Big(H_{\mathrm{LOS}} + \sum_{\iota} H_{\mathrm{ref},\iota}\Big)P_t. \tag{4}$$

C. MODELING USER MOBILITY

An important point here is to consider the effect of user mobility. For instance, it was shown in [45] that the quality of an RF-based extra-WBAN link is significantly affected by users' mobility. A variety of mobility models have been proposed so far in the context of cellular mobile networks such as random walk model [46], RWP [31], [32], random group model [47]–[49], and random trip model [50]. In the context of RF extra-WBANs, a modified RWP, called random room mobility model, was proposed in [45] for the case of mobility within a hospital building. Moreover, [51] showed that the human walk nature in outdoor follows the levy-walk model. In indoor environments, RWP is the most widely used mobility model because of being more realistic and its implementation simplicity [52]. In the case of OWC, in addition to user mobility, the effect of Tx orientation on the link performance can be quite significant. Recently, an ORWP mobility model was proposed for the light fidelity (LiFi) use cases, where mobile devices were considered to be oriented randomly with a Gaussian distribution [33]. Although in our case of extra-WBAN link, the Tx (placed on the patient's shoulder) would have smaller orientation variations, compared to the case of handheld devices in LiFi applications, here for the sake of modeling simplicity, we also consider the Gaussian distribution and use it in our ORWP mobility model.

1) TX ORIENTATION

The orientation of a Tx placed on a patient's shoulder can be described by the Euler's rotation theorem [53]. We denote the yaw, pitch, and roll angles by α, β, and γ, respectively. Let's define the reference coordinate system XYZ, corresponding to when the Tx is pointing straight towards the ceiling, in contrast to the actual coordinate system $x'y'z'$, see Fig. 4. Any spatial orientation can be represented by a 3×3 rotation matrix $\boldsymbol{R}$ given by [54]:

$$\boldsymbol{R} = \boldsymbol{R}_{\mathrm{yaw}}(\alpha)\boldsymbol{R}_{\mathrm{pitch}}(\beta)\boldsymbol{R}_{\mathrm{roll}}(\gamma) = \begin{bmatrix} \cos\alpha & -\sin\alpha & 0 \\ \sin\alpha & \cos\alpha & 0 \\ 0 & 0 & 1 \end{bmatrix} \times \begin{bmatrix} 1 & 0 & 0 \\ 0 & \cos\beta & -\sin\beta \\ 0 & \sin\beta & \cos\beta \end{bmatrix} \begin{bmatrix} \cos\gamma & 0 & \sin\gamma \\ 0 & 1 & 0 \\ -\sin\gamma & 0 & \cos\gamma \end{bmatrix}, \tag{5}$$

where $\boldsymbol{R}_{\mathrm{yaw}}$, $\boldsymbol{R}_{\mathrm{pitch}}$ and $\boldsymbol{R}_{\mathrm{roll}}$ are the rotation matrices about the Z, X and Y axes with rotation angles α, β, and γ, respectively. Let us define the normal vectors $\boldsymbol{n}_{\mathrm{Tx}} = [n_x n_y n_z]^T$ and $\boldsymbol{n}'_{\mathrm{Tx}} = [n'_x n'_y n'_z]^T$ corresponding to before and after Tx

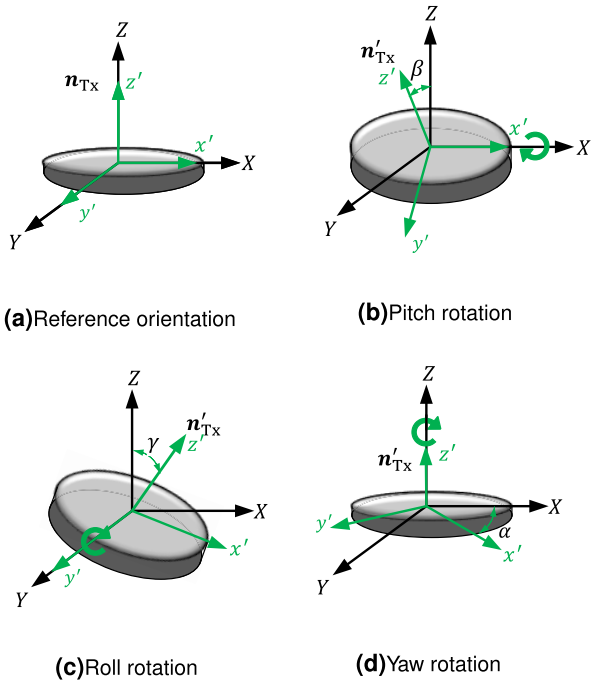

FIGURE 4. Orientations of a Tx: (a) reference orientation, when the reference coordinate system *XYZ* and the actual Tx coordinate system $x'y'z'$ are aligned, (b) Pitch rotation, the Tx rotation around the *X* axis with angle β, (c) Roll rotation, the Tx rotation around the *Y* axis with angle γ, (d) Yaw rotation, the Tx rotation around the *Z* axis with angle α.

rotation, respectively. According to the Euler's theorem,

$$\boldsymbol{n}'_{\mathrm{Tx}} = \boldsymbol{R}\,\boldsymbol{n}_{\mathrm{Tx}}. \tag{6}$$

We assume that the reference and the actual Tx coordinate systems are initially aligned so that $\boldsymbol{n}_{\mathrm{Tx}} = [0\,0\,1]^T$, see Fig. 4a. Then, substituting $\boldsymbol{R}$ from (5) in (6), we have:

$$\boldsymbol{n}'_{\mathrm{Tx}} = \begin{bmatrix} \sin\alpha\ \sin\beta\ \cos\gamma + \cos\alpha\ \sin\gamma \\ \sin\alpha\ \sin\gamma - \cos\alpha\ \cos\gamma\ \sin\beta \\ \cos\beta\ \cos\gamma \end{bmatrix}. \tag{7}$$

Now, we convert the rectangular coordinates to spherical coordinates as shown in Fig. 3 to obtain the elevation θ_{tx} and the azimuth ω_{tx} angles as follows:

$$\theta_{tx} = \arccos\left(\cos\beta\ \cos\gamma\right) \tag{8}$$

$$\omega_{tx} = \arctan\left(\frac{\sin\alpha\ \sin\gamma - \cos\alpha\ \cos\gamma\ \sin\beta}{\sin\alpha\ \sin\beta\ \cos\gamma + \cos\alpha\ \sin\gamma}\right). \tag{9}$$

Note that the radiance angle ϑ in Fig. 3 depends on the elevation θ_{tx} and the azimuth ω_{tx} angles, and can be calculated by employing the trigonometry of the rectangular triangles.

2) ORWP MODEL

According to the RWP mobility model, within a rectangular room of area $W \times L$, the distance between two random points is assumed to be distributed uniformly with the probability density function (PDF) $\frac{1}{WL}$ [55]. For the transition between two successive points, the trajectory is a straight path with a constant speed. The PDF of the distance or the transition length between two points, denoted by S can be found in [55].

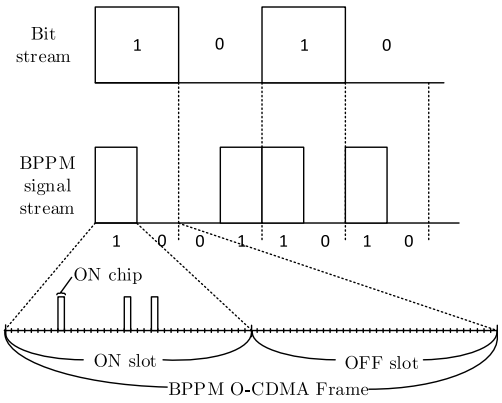

FIGURE 5. Example of frame structure of BPPM O-CDMA signaling.

For the case of an $L \times L$ square room that we consider here, the expected transition length is $E\{S\} = 0.5214\ L$ [55], [56]. The two dimensional PDF of the node location (x, y) is then [56]:

$$f_{XY}(x, y) = \frac{36}{L^6}\left(x^2 - L^2/4\right)\left(y^2 - L^2/4\right). \tag{10}$$

Here, we assume that the speed of the node (i.e., the user) is uniformly distributed between $V_{\min}$ and $V_{\max}$, which is considered to be unchanged during each transition. Then, the expected value of the transition time $\mathcal{T}$ is [56]:

$$E\{\mathcal{T}\} = \frac{\ln(V_{\max}/V_{\min})}{V_{\max} - V_{\min}} E\{S\}. \tag{11}$$

We consider the user movements with a certain amount of pause time $\mathcal{T}_p$ with the probability of pause, $P_{\text{Pause}} = E\{\mathcal{T}_p\}/(E\{\mathcal{T}_p\} + E\{\mathcal{T}\})$ [56]. The random location of the paused nodes is assumed to be uniformly distributed with the PDF $f_{XY}^{\text{Pause}}(x, y) = \frac{1}{WL}$. The global PDF of the node location taking into account the pause feature will be then:

$$f_{XY}^{\text{Global}} = P_{\text{Pause}} f_{XY}^{\text{Pause}}(x, y) + (1 - P_{\text{Pause}}) f_{XY}(x, y), \tag{12}$$

where $f_{XY}(x, y)$ corresponds to (10).

Now, to simulate the general ORWP mobility for a given user, for each waypoint, we consider an independently generated random Tx orientation to the user's location using (12).

D. O-CDMA SIGNALING

An illustrative example of a BPPM O-CDMA transmitted signal is shown in Fig. 5. Each user is assigned a signature code (SC), also called spread sequence, which is multiplied by the corresponding signal. At the Rx (i.e., the AP), signals of all users are received on the PD, see Fig. 6. In order to extract and detect the data of a specific user, each BPPM slot of the received signal is correlated with the corresponding SC (block "Correlator") over the slot duration. Afterwards, the demodulator extracts the transmitted bits by comparing the correlator outputs corresponding to the BPPM slots.

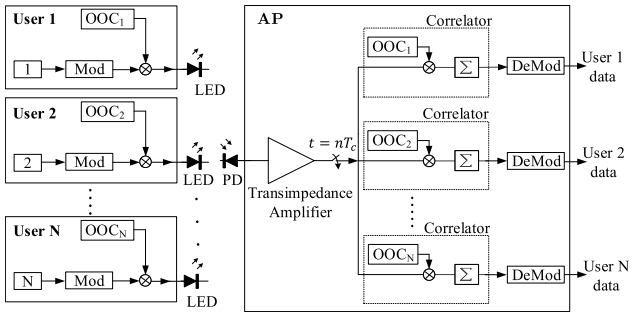

FIGURE 6. Block diagram of the proposed O-CDMA based extra-WBAN system; Blocks Mod and DeMod stand for modulator and demodulator. Signal sampling at the trans-impedance amplifier output is done at sampling period of T_c, the chip duration.

As explained previously, an OOC is usually used as SC. This binary sequence, is denoted by OOC$(F, K, \lambda_a, \lambda_c)$, where F is the SC length (i.e., the number of chips), K is its weight (i.e., the number of ones in the sequence), and λ_a and λ_c stand for the auto-correlation and cross-correlation constraints, respectively [57]. For given OOCs u and v, the following conditions hold [16]:

$$\Gamma_{u,u}(\kappa) = \sum_{n=0}^{F-1} u_n u_{n+\kappa} \begin{cases} = K & ; \ \kappa = 0 \\ \leq \lambda_a & ; \ 1 \leq \kappa \leq F-1 \end{cases} \tag{13}$$

$$\Gamma_{u,v}(\kappa) = \sum_{n=0}^{F-1} u_n v_{n+\kappa} \leq \lambda_c \ ; \ \ 0 \leq \kappa \leq F-1. \tag{14}$$

Here, $\Gamma_{u,u}$ and $\Gamma_{u,v}$ denote the auto-correlation of u, and the cross-correlation of u and v, respectively. As a matter of fact, since IM/DD signal transmission is used, here we cannot have strict orthogonality between two SCs. For OOCs, we have $\lambda_a = \lambda_c = 1$ which results in minimum MAI. For OOC$(F, K, 1, 1)$ codes, the maximum number of users N that can be handled is upper bounded by [16]:

$$N \leq \frac{F-1}{K(K-1)}. \tag{15}$$

For such codes, error-free data recovery for an "ideal" link (i.e., without noise effect and only from a MAI point of view) is possible provided that K satisfies the following condition [16], [57]:

$$K > N - 1. \tag{16}$$

Note that, the effect of MAI can be reduced when using M-ary PPM, $M > 2$ [58]. This, however, results in relatively poor bandwidth efficiency and increases the complexity of signal transmission at both Tx and Rx and the required speed of electronics. Therefore, we consider the BPPM modulation in this work, as mentioned previously. Note that, here, each BPPM slot duration equals $F T_c$.

III. PERFORMANCE EVALUATION OF BPPM O-CDMA SIGNALING

To study the performance of BPPM O-CDMA signaling for an extra-WBAN link, we consider two criteria of BER and P_{out}. We mostly focus on the latter as a more appropriate metric for a randomly changing channel. It is defined as the probability that the BER for a given channel realization exceeds a target value, BER_{th}:

$$P_{\text{out}} = P(\text{BER} \geq \text{BER}_{\text{th}}). \tag{17}$$

As mentioned previously, from a system design point of view, we consider asynchronous transmission from different users, which results in reduced implementation complexity. That is, each CN sends its data asynchronously to the AP. We are hence concerned by the near-far problem, which has been the subject of extensive research for CDMA-based RF systems [13], [59], e.g., in the context of the 3rd generation of cellular mobile networks. Here, in order to simplify the system performance analysis, we make the assumption of chip synchronous transmission. This corresponds the worst case, regarding MAI, and provides an upper bound on the system performance [60].

A. BER ANALYSIS

As shown in Fig. 5, BPPM symbols are composed of two ON and OFF slots. Here, without loss of generality, we assume that '0' and '1' information bits are mapped to (OFF, ON) and (ON, OFF) BPPM symbols, respectively. With BPPM O-CDMA, each slot of a given user is multiplied by its SC code, as illustrated in Fig. 5. For the synchronous transmission case, the ON chips of two OOCs (satisfying $\lambda_a = \lambda_c = 1$) cannot overlap on more than one chip position. For two different users, there are K^2 possible ways of overlapping between K ON chips of the two corresponding OOCs. Then, given the OOC length F, the probability that an interfering user's ON chips of a BPPM slot overlap with those of a desired user is given by [16], [26]:[1]

$$q = \frac{K^2}{2F}, \tag{18}$$

where the factor 1/2 is the probability that the interfering user sends a one in the first BPPM slot and a zero in the second BPPM slot. For a total number of N users, the probability $P_i(\ell)$ that ℓ users interfere with a desired user's signal follows a binomial distribution that can be expressed as [16], [60]:

$$P_i(\ell) = \binom{N-1}{\ell} q^{\ell} (1-q)^{N-1-\ell}; \quad 1 \leq \ell \leq N-1. \tag{19}$$

The overall probability of interference occurrence P_i is then:

$$P_i = \sum_{\ell=1}^{N-1} P_i(\ell); \quad 1 \leq \ell \leq N-1, \tag{20}$$

and we consider $P_i = 1$ for $\ell = 0$. The first step of the decoding process is to correlate the received signal with the corresponding OOC code over the BPPM slot duration. Let us denote by χ_1 and χ_2 the correlator outputs corresponding to

[1] Note that the probability of interference between two OOCs with either OOK or BPPM modulations is the same [26].

the first and the second BPPM slots, respectively. For demodulation, these outputs are compared to make a decision on the transmitted bit (the DeMod block in Fig. 6). A detection error occurs if $\chi_2 > \chi_1$, when the transmitted data bit is '1', or if $\chi_1 > \chi_2$, otherwise. Assuming equally likely transmitted bits, the bit error probability P_E, or in other words the BER, is given by [61]:

$$\begin{aligned} P_E &= \frac{1}{2}P_i\Big[P_E(\text{error}|'0') + P_E(\text{error}|'1')\Big] \\ &= \frac{1}{2}P_i\Big[\text{Prob}(\chi_1 \geq \chi_2|'0') + \text{Prob}(\chi_2 \geq \chi_1|'1')\Big], \end{aligned} \quad (21)$$

where 1/2 is the probability of the transmitted bit '1' or '0' and, for instance, $P_E(\text{error}|'0')$ denotes the error probability conditioned to the transmission of a bit '0'. Logically, we have $P_E(\text{error}|'0') = P_E(\text{error}|'1')$.

To analyze the worst MAI case, in addition to the assumption of synchronous chip transmission, we consider the case where the desired user transmits a bit '0', represented by the (OFF, ON) BPPM symbol, and all the $N-1$ interferers transmit bit '1', i.e., the (ON, OFF) BPPM symbol. This allows to evaluate the upper bound on the conditional probability. Concerning the Rx noise, the corresponding generated photoelectrons at the PD output over an O-CDMA chip time T_c has a Poisson distribution [62]. Concerning the correlator output at each BPPM slot, the resulting Poisson distribution with a relatively large mean can be well approximated by a Gaussian distribution. Let us denote by I_1 and I_2, and σ_1^2 and σ_2^2, the means and variances of the correlator outputs corresponding to the first and second BPPM slots, respectively. We have:

$$\begin{aligned} I_1 &= KI_d + KI_a + \sum_{j=1}^{N-1} I_{Ij}, \\ I_2 &= KI_d + KI_a + KI_r, \\ \sigma_1^2 &= K\sigma_{I_d}^2 + K\sigma_{I_a}^2 + \sum_{j=1}^{N-1} \sigma_{I_{Ij}}^2 + K\sigma_T^2, \\ \sigma_2^2 &= K\sigma_{I_d}^2 + K\sigma_{I_a}^2 + K\sigma_{I_r}^2 + K\sigma_T^2. \end{aligned} \quad (22)$$

Here, I_d and I_a denote the dark current noise and the ambient current noise, I_r is the photo-current corresponding to the desired user's chip, and I_{Ij} is the photo-current corresponding to the j^{th} interfering user's ON chips. The factor K in I_1 and I_2 is due to the correlation with the OOC, which has weight K. We have:

$$I_r = \frac{q_e\,\eta\,P_r}{h\,\nu}, \quad I_{Ij} = \frac{q_e\,\eta\,P_{r,j}}{h\,\nu}, \quad (23)$$

where ν is the light frequency, η is the PD quantum efficiency, and h is the Plank's constant. Also, P_r is the received power from the desired user and $P_{r,j}$ is the received power from the j^{th} interferer. The corresponding variances are [63]:

$$\begin{cases} \sigma_{I_d}^2 = 2\,q_e\,I_d\,B, \\ \sigma_{I_a}^2 = 2\,q_e\,I_a\,B, \\ \sigma_{I_r}^2 = 2\,q_e\,I_r\,B, \\ \sigma_{I_{Ij}}^2 = 2\,q_e\,I_{Ij}\,B. \end{cases} \quad (24)$$

Here, B denotes the bandwidth of the Rx low-pass filter and q_e is the electron charge. Also, σ_T^2 in (22) stands for the Rx thermal noise variance, defined as [63]:

$$\sigma_T^2 = \frac{4\,K_B\,T_r\,B}{R_L}, \quad (25)$$

where T_r is the equivalent noise temperature, K_B denotes Boltzman's constant and R_L is the load resistance of the Rx trans-impedance amplifier (TIA).

Note that, given that the correlation with the OOC consist of the summation of signals corresponding to non-zero weights, the noise at the correlator output can be assumed to follow a Gaussian distribution. Consequently, we can write [61]:

$$\begin{aligned} \text{Prob}(\chi_1 \geq \chi_2|'0') = &\int_{-\infty}^{\infty} \frac{1}{\sqrt{2\pi\sigma_1^2}} \exp^{-(x-I_1)^2/2\sigma_1^2} \\ &\times \int_{-\infty}^{x} \frac{1}{\sqrt{2\pi\sigma_2^2}} \exp^{-(y-I_2)^2/2\sigma_2^2}\,dy\,dx, \end{aligned} \quad (26)$$

The BER for the case of the absence of MAI can be calculated by setting $\ell = 0$ in (19) and $P_{r,j} = 0$ in (23).

IV. PERFORMANCE ANALYSIS

We present here a set of numerical results to study the performance of an extra-WBAN link using BPPM O-CDMA signaling. Simulation parameters are summarized in Table 1. In particular, to reduce the probability of LOS blockage, we consider a relatively wide beam at the Tx, i.e., $\phi_{1/2} = 60°$ corresponding to $m = 1$, and a relatively large Rx FOV, i.e., $\psi_c = 75°$. Also, by default and unless otherwise mentioned, one single AP is considered, placed at the center of the ceiling. Note that the body has a rather little impact on the link performance for relatively low data-rate applications, provided that the P_{out} requirement is limited to about 10^{-2} [64]. Therefore, to simplify channel modeling and to reduce the simulation time, the impact of the patient's body is not taken into account in our study, assuming that a P_{out} of 10^{-2} would be adequate to achieve the required quality-of-service for the considered WBAN applications.

A. EFFECT OF TX ORIENTATION ON THE RECEIVED POWER

Let us first consider a single Tx in the room, i.e., the case of no MAI, and see the effect of random orientations of the Tx. As a link outage can most possibly occur due to LOS blockage, we study the effect of Tx random orientations on the received power by neglecting the diffuse link. Figure 7 shows the received optical power at the AP versus $-90° \leq \theta_{tx} \leq 90°$ for different Tx distances d from the room

TABLE 1. Parameters Used for Numerical Simulations.

Parameter	Symbol	Value
Max. number of users	N	4
Transmission bandwidth	B	10 MHz
Target BER	BER_{th}	10^{-3}
Room dimension	—	$8 \times 8 \times 3\,\text{m}^3$
CN height	h_2	1.4 m
Tx orientation angle	θ_{tx}	-90° – 90°
Walls reflection coefficient [65]	ρ	0.8
No. of reflecting surface elements	—	100 /m^2
Patient minimum speed	$V_{\min}$	0.2 m/s
Patient maximum speed	$V_{\max}$	0.6 m/s
Pause time	$\mathcal{T}_p$	1 sec
LED wavelength	λ	880 nm
LED semiangle at half power [14]	$\phi_{1/2}$	60°
OOC code	—	(49,4,1,1)
OOC length	F	49
OOC weight	K	4
PD quantum efficiency [66]	η	0.66
PD active area	A_d	1 cm^2
TIA load resistance	R_L	10 kΩ
Rx dark current [67]	I_d	10 nA
Rx noise temperature	T_r	300 K
Rx FOV	ψ_c	75°
Ambient current noise [68]	I_a	490 μA

center assuming a 100 mW transmit power. As seen from the figure, for too large θ_{tx}, the LOS between the Tx and the AP is lost, resulting in zero received power (remember that we neglect the diffuse link). For $d = 0$, the received power falls to zero for $|\theta_{tx}|$ larger than the Rx FOV. Logically, random orientation of the CN can have a more detrimental impact on the link performance as the Tx moves from the center of the room to the corner. For instance, for $d = 3.5$ m, the LOS is lost for $\theta_{tx} > 8°$ only.

Let us now consider the effect of Tx random orientation $-90° \leq \theta_{tx} \leq 90°$ on the detected received optical power at the AP. We have presented in Fig. 8 the minimum and maximum detectable received power versus d, considering the cases of LOS and LOS+1$^{\text{st}}$-order reflections and for different transmit power levels P_t. As expected, the minimum and maximum received powers decrease with increasing d when taking only the LOS into account. However, when taking the 1$^{\text{st}}$-order reflections into account, the maximum received power increases slightly as the distance d increases due to the decreasing path length of the first-order reflections from the walls.

B. MAI EFFECT ON LINK PERFORMANCE

To focus on the MAI effect, we again consider only the LOS link by neglecting the diffuse link. We start by considering some special scenarios for a desired user and three

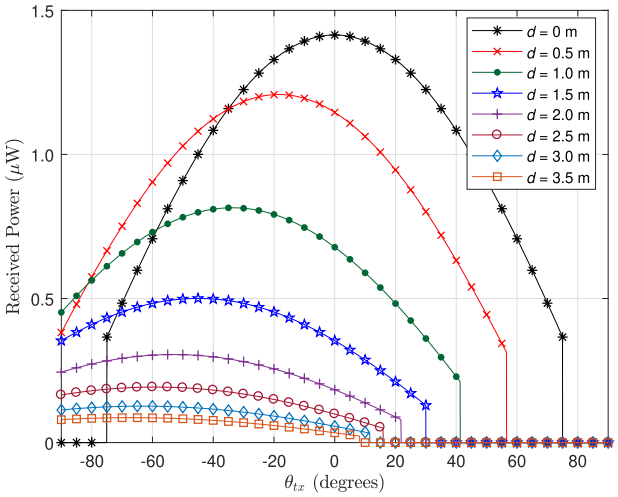

FIGURE 7. Impact of Tx orientation on the LOS outage for distances *d* from the room center, $P_t = 100$ mW. Only the LOS path is taken into consideration.

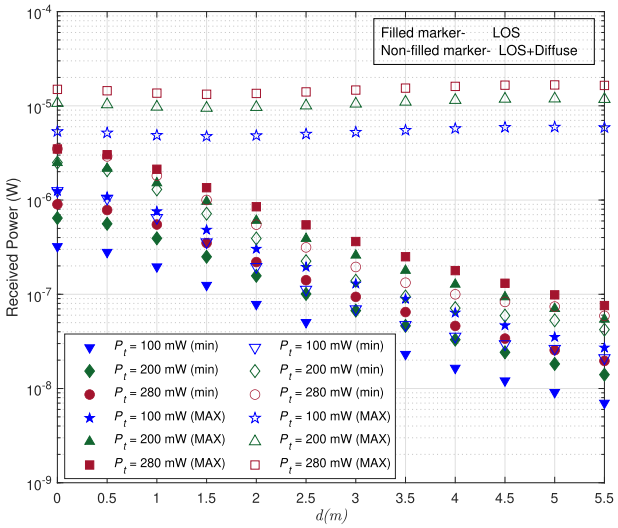

FIGURE 8. Impact of Tx orientation on the minimum (min) and maximum (MAX) detectable received power for distances *d* from the room center. LOS and LOS+1$^{\text{st}}$-order reflections are taken into consideration.

interfering users. First, we consider the scenario where all the three interferers are at the same position at the room center, and change the desired user's position from $d = 0$ to 5.7 m, i.e., from the center of the room to the corner, as shown in Fig. 9. These two positions correspond to the least and most MAI, respectively.

B.1. FIXED TX ORIENTATION

At first, we assume that all Txs are oriented towards the ceiling i.e., $\theta_{tx} = 0$, regardless of their position. For a given d, the BER is calculated from (21). The BER plots of the desired user are presented in Fig. 10 for different transmit power levels P_t, which is set equal for all users. As expected, the BER increases as the desired user moves towards the room corner, where it undergoes the worst MAI due to the so-called near-far problem. At the most favorable position, i.e., at the

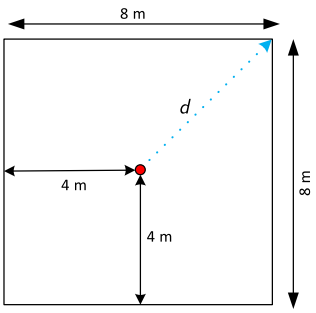

FIGURE 9. Trajectory of the displacement of the desired user from $d = 0$ (room center) to $d = 5.7$ m (room corner).

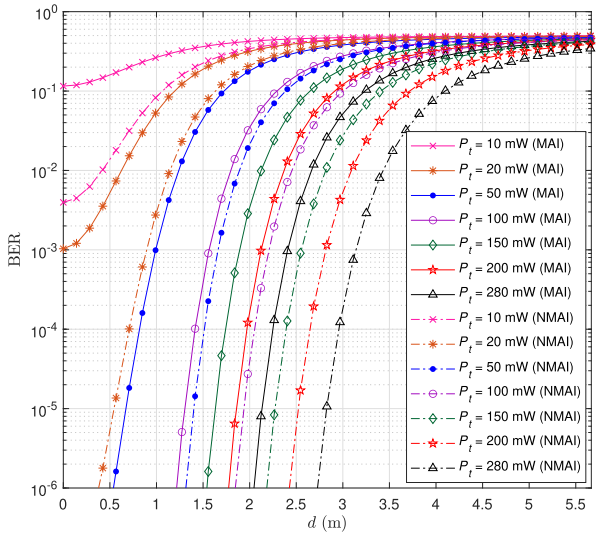

FIGURE 10. BER versus the horizontal distance d of the desired user from the AP for different transmit powers. MAI represents the case where the three other users are located at the same position at the room center. NMAI stands for no-MAI. Only the LOS path is taken into consideration.

room center $d = 0$, the link performance is practically limited by the least MAI (with no near-far problem) and noise. As expected, a better performance is obtained by increasing the transmit power. As benchmark, and in order to elucidate the MAI effect, we have also shown in Fig. 10 the BER plots for the no-MAI case, denoted by NMAI. Note that, for NMAI case, the increase in BER with d is due to decrease in the received signal-to-noise ratio (SNR), as it can be seen in Fig. 7 for $\theta_{tx} = 0$.

B.2. RANDOM TX ORIENTATION

Now we consider the effect of random Tx orientation for the same scenario as in the previous subsection. For this, we generate for every user 10^6 Gaussian-distributed random values for yaw α, pitch β, and roll γ angles in the intervals of (-180°, 180°), (-60°, 60°) and (-60°, 60°), respectively. Given the random channel, we consider as performance metric the outage probability P_{out}, calculated considering $\text{BER}_{\text{th}} = 10^{-3}$. The P_{out} plots are presented in Fig. 11 for different transmit powers P_t. As expected, P_{out} increases as the desired user

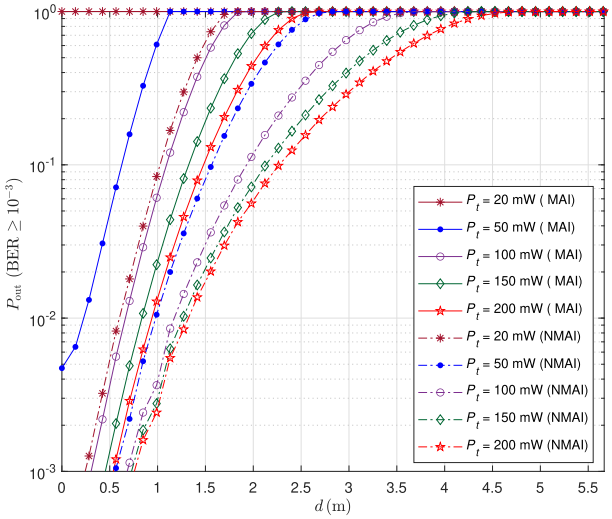

FIGURE 11. Outage probability versus the horizontal distance of the desired user from the AP for different transmit powers. MAI represents the case where the three other users are located at the same position at the room center. The three interferers and the desired user are oriented randomly at their positions. Only the LOS path is taken into consideration.

moves from the center of the room to the corner since there is a higher probability of losing the LOS, see Fig. 7. In fact, at the center, the performance is mainly affected by decreased SNR due to random orientations of the Tx, as shown in Fig. 8. Again, with increased P_t, a lower P_{out} is achieved for both MAI and NMAI scenarios. However, almost the same results are obtained for $P_t \geq 200$ mW (results are not shown for the sake of presentation clarity), which means that the limiting factor resulting in link outage is LOS blockage (rather than decreased SNR).

B.3. ACCOUNTING FOR NON-LOS CONTRIBUTION

So far, to show the impact of Tx orientation, we only considered LOS contribution to signal propagation. We now take into account non-LOS propagation by considering 1st-order reflections, which correspond to the major contribution from diffuse propagation. Higher-order reflections are neglected to avoid considerably increased simulation time. We consider that each wall is composed of a set of Lambertian reflecting surface elements, with 100 elements per square meter, which is sufficient for accurate channel estimation [69], [70].

We have shown the resulting P_{out} plots in Fig. 12 for the same scenarios as in Fig. 11. We can notice the significant difference between the results of these two figures which signifies the substantial role of the diffuse link in the case of LOS blockage due to random Tx orientations. For instance, for $P_t = 50$ mW at $d = 1$ m and MAI case, P_{out} is around 0.6 from Fig. 11, whereas it is lower than 0.05 from Fig. 12. We also notice a leveling effect in P_{out} as d increases, irrespective of P_t. This is due to the fact that the power received from the first-order reflections increases with increasing d, as the corresponding path length (reflections from walls) decreases, whereas the probability of LOS blockage increases (as shown in Figs. 7 and 8). Note that at the extreme room corner,

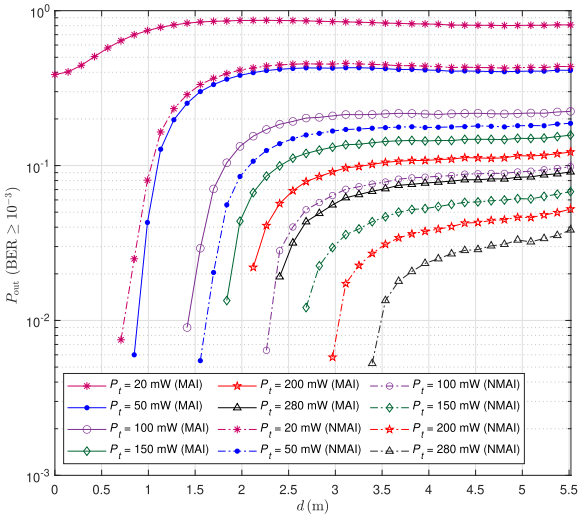

FIGURE 12. Outage probability versus the horizontal distance of the desired user from the AP, taking into account LOS and 1st-order reflections. MAI represents the case where the three other users are located at the same position at the room center. The three interferers and the desired user are oriented randomly at their positions.

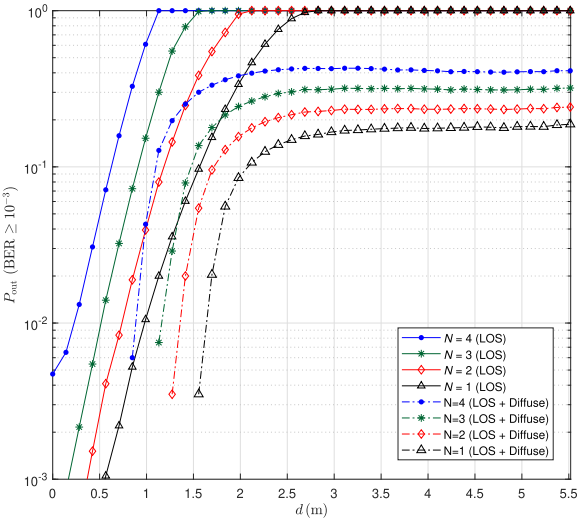

FIGURE 13. Outage probability versus the horizontal distance of the desired user from the AP for different numbers of users N. Interferers are located at the same position at the room center. $P_t = 50$ mW. The three interferers and the desired user are oriented randomly at their positions.

the calculated P_{out} from the simulations steeply increases to one, which is due to considering only 1st-order reflections in our simulations. To obtain more accurate simulations, higher-order reflections need to be taken into account, which will considerably increase the simulation time. Nevertheless, such user positions are very unlikely to occur in practice, due to the user's body volume. For this reason, we have excluded these values ($d \gtrsim 5.5$ m) in Fig. 12 and the subsequent figures.

In order to better see the impact of MAI, we have shown in Fig. 13 P_{out} plots versus d for different numbers of users N, for $P_t = 50$ mW and the MAI configuration as in Figs. 11 and 12, taking into account both LOS and LOS+1st-order reflections. Note that, $N = 1$ corresponds to NMAI case. As expected, P_{out} degrades with increased number of interferers.

B.4. ACCOUNTING FOR RANDOM USER MOVEMENTS

Up to now, we considered fixed interferers' positions (in the center of the room, i.e., the worst MAI case) to better see the impact of MAI and random Tx orientations. In order to investigate the actual effect of MAI in a more practical scenario, we consider now randomly moving interferers according to the ORWP model (see Section II) for a given position of a desired user. The speed variation interval and the pause time for the ORWP model are specified in Table 1. As before, we change the position of the desired user from the center of the room to the corner. Results are presented in the Fig. 14, where we have generated 10^6 random positions of the interferers, as well as 10^6 random orientations for the main user and the interferers. Compared with the case in Fig. 12, here we observe a slightly less destructive MAI effect on the desired user's link performance. This could be expected as in the present case, we consider randomly moving interferers where the MAI effect will be less significant overall,

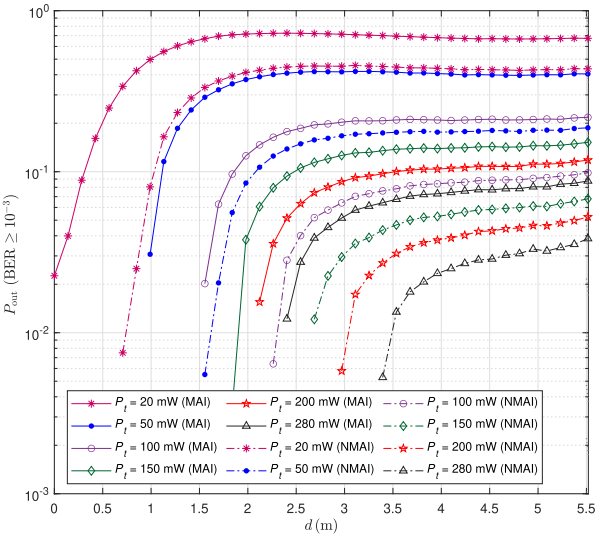

FIGURE 14. Outage probability versus the horizontal distance of the desired user from the AP, taking into account LOS and 1st-order reflections. The three interferers are randomly moving and oriented based on the ORWP mobility model inside the room; the desired user is randomly oriented at each position.

in particular, for relatively small d. Also, the worst MAI case in Fig. 12 (where the interferers and the desired user are all located at the room center) does not happen here since the interferers are considered to move randomly in the room.

C. INTEREST OF USING MULTIPLE APs

So far we showed how significantly the existence of a LOS between the Tx and the AP can improve the link performance. Indeed, we concluded that link outages mostly occur due to Tx random orientations, where the LOS is lost and the received signal (from reflections) is too weak. One efficient technique to reduce this "fading" effect is to employ spatial diversity by using multiple APs. To evaluate the obtained

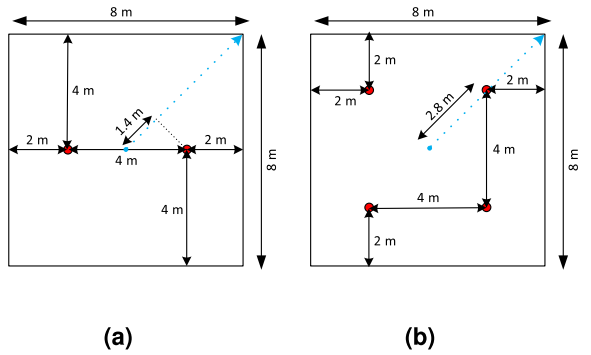

FIGURE 15. Arrangements of APs on the ceiling for the room size $(8 \times 8 \times 3)\ \mathrm{m}^3$: (a) case of 2 APs, (b) 4 APs. Here, dotted blue line represents the horizontal distance d from the center of the room.

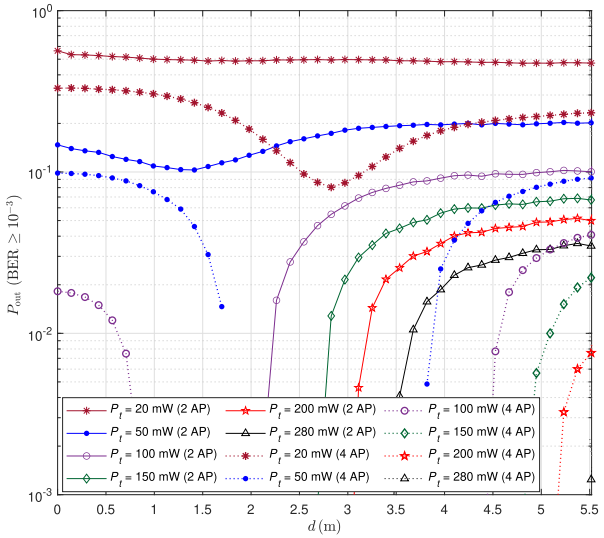

FIGURE 16. Outage probability versus the horizontal distance of the desired user from the center of the room for the 2 and 4 AP configurations, considering LOS+1st-order reflections. Three randomly moving and oriented interferers based on the ORWP mobility model; randomly oriented desired user at each position.

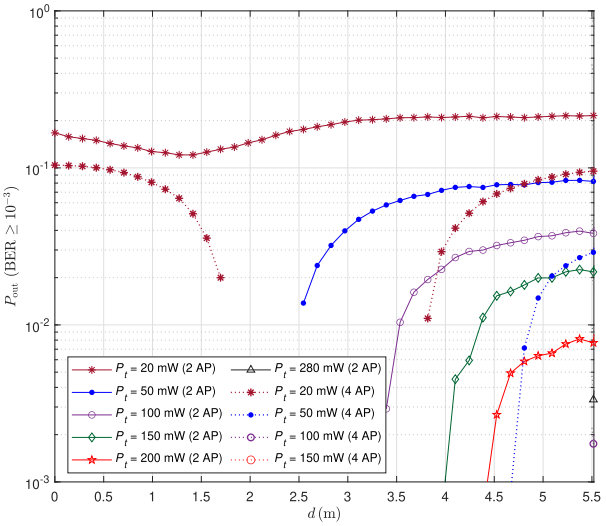

FIGURE 17. Outage probability versus the horizontal distance of the desired user from the center of the room for the 2 and 4 AP configurations for the case of NMAI. The desired user is oriented randomly at each position. LOS+1st-order reflections are considered.

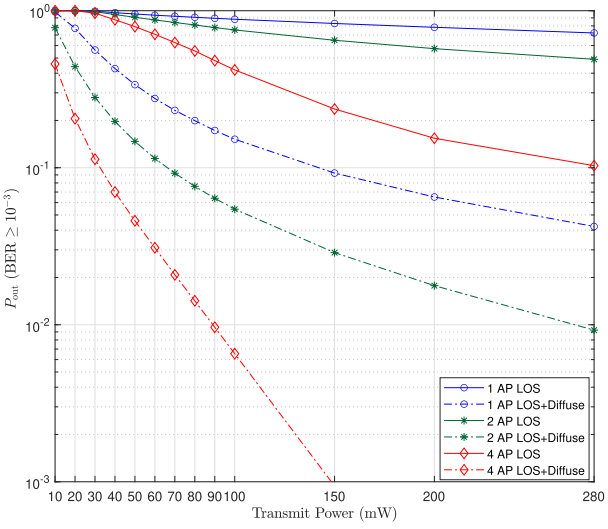

FIGURE 18. Outage probability versus the transmit power P_t with randomly moving and oriented desired user and interferers for the cases of one, two, and four APs based on the ORWP mobility model. Two cases of LOS and LOS+ 1st-order reflections are considered.

performance improvement, we consider the case of two and four APs placed symmetrically on the ceiling, as shown in Fig. 15. We perform equal gain combining (EGC) on the signals received on the APs, assuming their perfect synchronization. Note that EGC provides performance close to the optimal maximal-ratio combining, while having a lower implementation complexity [13]. The assumption of perfect time synchronization is quite logical in this context: considering a maximum data-rate of 100 Kbps and the OOC code length of 49, the slot duration of the BPPM O-CDMA signal is about 100 ns. So, even a path length difference of 5 m between the Tx and the two APs in Fig. 15(a) would result in a maximum delay difference of about 15 ns, which can be effectively neglected.

We have presented the P_{out} plots in Figs. 16 and 17 for the cases of 2 and 4 APs with and without MAI, respectively. By comparing these results with Fig. 14, we notice firstly that for relatively large d where the P_{out} degrades due to low received signal power, here spatial diversity helps improve the signal quality and the link P_{out}. Here, as illustrated in Fig. 15, the shortest distance between the desired Tx and an AP is $d \approx 1.4$ and 2.8 m for the cases of 2 and 4 APs, respectively, at which we notice the lowest P_{out} for a given P_t. Therefore, as the desired user moves from the center of the room to the corner, P_{out} decreases at first, due to the decreasing distance between the Tx and an AP. Then, as the distance between the Tx and the AP increases, P_{out} increases. This explains the non-monotonic trend of P_{out} plots in Figs. 16 and 17 with d. Note that as explained previously in Subsection IV-B3, the results at the extreme corner are excluded from these figures.

Lastly, we consider a realistic scenario where all users move randomly according to the ORWP model (with random

speed and pause time) inside the room and random Tx orientations. P_{out} plots are presented in Fig. 18 for different P_t and for the cases of 1, 2, and 4 APs when only LOS or LOS and 1$^{\text{st}}$-order reflections are considered for signal propagation. The interesting result is that the contribution of the diffuse link (i.e., non-LOS) becomes much more significant by increasing the number of APs. It is quite marginal for the case of a single AP, which is consistent with the results of Fig. 14. This substantial improvement for the case of multiple APs can be explained by a globally shorter path length to at least one AP from the 1$^{\text{st}}$-order reflection when the LOS is lost.

V. CONCLUSION AND FUTURE WORK

We investigated the performance of BPPM O-CDMA based uplink extra-WBAN signal transmission for multi-user medical applications. We studied the impact of Tx orientation and changing positions of the users (both the desired user and the interferers) with respect to the AP, according to a realistic ORWP mobility model, and evaluated the effect of MAI on a desired user performance. For this, we considered two cases where only the LOS or the LOS plus 1$^{\text{st}}$-order reflections were taken into account. In our analysis, for the sake of simplicity of analytical derivations, we considered the case of chip synchronous transmission, which corresponds the worst MAI conditions.

We showed that random Tx orientations have a more detrimental effect on the link performance (i.e., link outage due to LOS blockage) as the distance between the AP and the CN increases. We showed the substantial improvement in the link performance by using several APs in the room, albeit the increased system implementation complexity. In the meanwhile, we elucidated the important contribution of the 1$^{\text{st}}$-order reflections in the link performance.

As a future research direction, it would be interesting to investigate the efficiency of using a HL device prior to the correlator, as suggested in [29], to reduce the MAI effect by limiting the interference level. Studying the practical interest of power control [17] at the Tx to reduce the near-far problem is another interesting direction for future work.

REFERENCES

[1] S. Movassaghi, M. Abolhasan, J. Lipman, D. Smith, and A. Jamalipour, "Wireless body area networks: A survey," *IEEE Commun. Surveys Tuts.*, vol. 16, no. 3, pp. 1658–1686, 3rd Quart., 2014.

[2] O. Haddad, M.-A. Khalighi, S. Zvanovec, and M. Adel, "Channel characterization and modeling for optical wireless body-area networks," *IEEE Open J. Commun. Soc.*, vol. 1, pp. 760–776, Jun. 2020.

[3] B. Latré, B. Braem, I. Moerman, C. Blondia, and P. Demeester, "A survey on wireless body area networks," *Wireless Netw.*, vol. 17, no. 1, pp. 1–18, Jan. 2011.

[4] O. Haddad and M. A. Khalighi, "Enabling communication technologies for medical wireless body-area networks," in *Proc. Global LIFI Congr. (GLC)*, Paris, France, Jun. 2019, pp. 1–5.

[5] O. Haddad, M. A. Khalighi, and S. Zvanovec, "Channel characterization for optical extra-WBAN links considering local and global user mobility," in *Proc. SPIE Photon. West, Broadband Access Commun. Technol. XIV*, vol. 11307, B. B. Dingel, K. Tsukamoto, and S. Mikroulis, Eds. San Francisco, CA, USA, 2020, pp. 89–97.

[6] Z. Ghassemlooy, L. N. Alves, S. Zvanovec, and M. A. Khalighi, Eds., *Visible Light Communications: Theory and Applications*. Boca Raton, FL, USA: CRC Press, 2017.

[7] *Photobiological Safety of Lamps and Lamp Systems*, IEC Standard 62471, International Electrotechnical Commission, Geneva, Switzerland, 2008.

[8] J. An, N. Q. Pham, and W.-Y. Chung, "Multiple bio-monitoring system using visible light for electromagnetic-wave free indoor healthcare," *Opt. Commun.*, vol. 405, pp. 107–113, Dec. 2017.

[9] D. R. Dhatchayeny, S. Arya, and Y. H. Chung, "Infrared-based multiple-patient monitoring in indoor optical wireless healthcare systems," *IEEE Sensors J.*, vol. 19, no. 14, pp. 5594–5599, Jul. 2019.

[10] G. Sun, K. Wang, H. Yu, X. Du, and M. Guizani, "Priority-based medium access control for wireless body area networks with high-performance design," *IEEE Internet Things J.*, vol. 6, no. 3, pp. 5363–5375, Jun. 2019.

[11] M. Hasan, M. Shahjalal, M. Chowdhury, and Y. Jang, "Real-time healthcare data transmission for remote patient monitoring in patch-based hybrid OCC/BLE networks," *Sensors*, vol. 19, no. 5, p. 1208, Mar. 2019.

[12] J. An and W.-Y. Chung, "Single-LED multichannel optical transmission with SCMA for long range health information monitoring," *J. Lightw. Technol.*, vol. 36, no. 23, pp. 5470–5480, Dec. 1, 2018.

[13] J. G. Proakis and M. Salehi, *Digital Communications*, 5th ed. New York, NY, USA: McGraw-Hill, 2007.

[14] J. M. Kahn and J. R. Barry, "Wireless infrared communications," *Proc. IEEE*, vol. 85, no. 2, pp. 265–298, Feb. 1997.

[15] D. In Kim, "Multi-user performance of direct-sequence CDMA using combined binary PPM/orthogonal modulation," *IEEE Trans. Commun.*, vol. 47, no. 3, pp. 404–415, Mar. 1999.

[16] J. A. Salehi, "Code division multiple-access techniques in optical fiber networks. I. Fundamental principles," *IEEE Trans. Commun.*, vol. 37, no. 8, pp. 824–833, Aug. 1989.

[17] R. Cameron and B. Woerner, "Performance analysis of CDMA with imperfect power control," *IEEE Trans. Commun.*, vol. 44, no. 7, pp. 777–781, Jul. 1996.

[18] J. R. Barry, E. A. Lee, and D. G. Messerschmitt, *Digital Communications*, 3rd ed. Berlin, Germany: Springer, 2012.

[19] J.-Y. Wang, Q.-L. Li, J.-X. Zhu, and Y. Wang, "Impact of receiver's tilted angle on channel capacity in VLCs," *Electron. Lett.*, vol. 53, no. 6, pp. 421–423, Mar. 2017.

[20] T. B. Hoang, S. Sahuguède, and A. Julien-Vergonjanne, "Optical wireless network design for off-body-sensor based monitoring," *Wireless Commun. Mobile Comput.*, vol. 2019, p. 13, Sep. 2019.

[21] B. Ghaffari, M. Matinfar, and J. Salehi, "Wireless optical CDMA LAN: Digital design concepts," *IEEE Trans. Commun.*, vol. 56, no. 12, pp. 2145–2155, Dec. 2008.

[22] B. Ghaffari, M. Matinfar, and J. Salehi, "Wireless optical CDMA LAN: Digital implementation analysis," *IEEE J. Sel. Areas Commun.*, vol. 27, no. 9, pp. 1676–1686, Dec. 2009.

[23] S. Zahedi, J. A. Salehi, and M. Nasiri-Kenari, "A photon counting approach to the performance analysis of indoors wireless infrared CDMA networks," in *Proc. 11th IEEE Int. Symp. Pers. Indoor Mobile Radio Commun. (PIMRC)*, London, U.K., vol. 2, Sep. 2000, pp. 928–932.

[24] S. L. Dhomeja, T. B. Oon, and R. Steele, "Performance of non-directed infrared CDMA," in *Proc. Int. Conf. Universal Pers. Commun.*, Florence, Italy, vol. 1, Oct. 1998, pp. 453–457.

[25] A. Aminzadeh-Gohari and M. R. Pakravan, "Analysis of power control for indoor wireless infrared CDMA communication," in *Proc. IEEE Int. Perform. Comput. Commun. Conf.*, Phoenix, AZ, USA, Apr. 2006, pp. 297–302.

[26] S. Khazraei and M. R. Pakravan, "Power control analysis for indoor wireless infrared CDMA networks using BPPM," in *Proc. IEEE Int. Conf. Telecommun. Malaysia Int. Conf. Commun.*, Penang, Malaysia, May 2007, pp. 402–406.

[27] N. Barbot, S. Sahuguede, and A. Julien-Vergonjanne, "Performance of a mobile wireless optical CDMA monitoring system," in *Proc. Int. Symp. Wireless Commun. Syst. (ISWCS)*, Paris, France, Aug. 2012, pp. 666–670.

[28] L. Chevalier, S. Sahuguéde, and A. Julien-Vergonjanne, "Wireless optical technology based body area network for health monitoring application," in *Proc. IEEE Int. Conf. Commun. (ICC)*, London, U.K., Jun. 2015, pp. 2863–2868.

[29] A. Julien-Vergonjanne, S. Sahuguède, and L. Chevalier, "Optical wireless body area networks for healthcare applications," in *Optical Wireless Communications: An Emerging Technology*, M. Uysal, C. Capsoni, Z. Ghassemlooy, A. Boucouvalas, and E. Udvary, Eds. Cham, Switzerland: Springer, 2016, pp. 569–587.

[30] M. J. Hasan, M. A. Khalighi, and B. Bechadergue, "Experimental implementation of Optical-CDMA for medical extra-WBAN links," in *Proc. Int. Symp. Commun. Syst., Netw. Digit. Signal Process. (CSNDSP)*, Jul. 2020, Porto, Portugal.
[31] D. B. Johnson and D. A. Maltz, *Dynamic Source Routing in Ad Hoc Wireless Networks*. New York, NY, USA: Springer, 1996, pp. 153–181.
[32] S. Althunibat, O. S. Badarneh, and R. Mesleh, "Random waypoint mobility model in space modulation systems," *IEEE Commun. Lett.*, vol. 23, no. 5, pp. 884–887, May 2019.
[33] M. D. Soltani, A. A. Purwita, Z. Zeng, H. Haas, and M. Safari, "Modeling the random orientation of mobile devices: Measurement, analysis and LiFi use case," *IEEE Trans. Commun.*, vol. 67, no. 3, pp. 2157–2172, Mar. 2019.
[34] M. Phiri, "Health building note 00-01. General design guidance for healthcare buildings," Dept. Health, Washington, DC, USA, Tech. Rep., 2014.
[35] *DS190 LUXEON IR Compact Line Product Datasheet*, Lumileds Holding B.V., San Jose, CA, USA, 2018.
[36] L. Chevalier, S. Sahuguède, and A. Julien-Vergonjanne, "Optical wireless links as an alternative to radio-frequency for medical body area networks," *IEEE J. Sel. Areas Commun.*, vol. 33, no. 9, pp. 2002–2010, Sep. 2015.
[37] R. Cavallari, F. Martelli, R. Rosini, C. Buratti, and R. Verdone, "A survey on wireless body area networks: Technologies and design challenges," *IEEE Commun. Surveys Tuts.*, vol. 16, no. 3, pp. 1635–1657, 3rd Quart., 2014.
[38] M. Patel and J. Wang, "Applications, challenges, and prospective in emerging body area networking technologies," *IEEE Wireless Commun.*, vol. 17, no. 1, pp. 80–88, Feb. 2010.
[39] F. Xu, M. A. Khalighi, and S. Bourennane, "Efficient channel coding for multipulse pulse position modulation in terrestrial FSO systems," in *Free-Space Laser Communications IX*, vol. 7464, A. K. Majumdar and C. C. Davis, Eds. Bellingham, WA, USA: SPIE, 2009, pp. 204–215.
[40] J. Abshire, "Performance of OOK and low-order PPM modulations in optical communications when using APD-based receivers," *IEEE Trans. Commun.*, vol. 32, no. 10, pp. 1140–1143, Oct. 1984.
[41] F. Xu, M.-A. Khalighi, and S. Bourennane, "Coded PPM and multipulse PPM and iterative detection for free-space optical links," *IEEE/OSA J. Opt. Commun. Netw.*, vol. 1, no. 5, pp. 404–415, Oct. 2009.
[42] Z. Ghassemlooy, W. Popoola, and S. Rajbhandari, *Optical Wireless Communications: System and Channel Modelling With MATLAB*, 2nd ed. Boca Raton, FL, USA: CRC Press, 2019.
[43] S. Long, S. Bourennane, M. Wolf, Z. Ghassemlooy, and M. A. Khalighi, "Investigating channel frequency selectivity in indoor visible-light communication systems," *IET Optoelectron.*, vol. 10, no. 3, pp. 80–88, Jun. 2016.
[44] Y. Qiu, H.-H. Chen, and W.-X. Meng, "Channel modeling for visible light communications—A survey," *Wireless Commun. Mobile Comput.*, vol. 16, no. 14, pp. 2016–2034, Oct. 2016.
[45] S. Misra, J. Mahapatro, M. Mahadevappa, and N. Islam, "Random room mobility model and extra-wireless body area network communication in hospital buildings," *IET Netw.*, vol. 4, no. 1, pp. 54–64, Jan. 2015.
[46] M. M. Zonoozi and P. Dassanayake, "User mobility modeling and characterization of mobility patterns," *IEEE J. Sel. Areas Commun.*, vol. 15, no. 7, pp. 1239–1252, Sep. 1997.
[47] P. Santi, *Mobility and Other Synthetic Mobility Models*. Hoboken, NJ, USA: Wiley, 2012.
[48] L. Tu, F. Zhang, F. Wang, and X. Wang, "A random group mobility model for mobile networks," in *Proc. Symposia Workshops Ubiquitous, Autonomic Trusted Comput.*, Brisbane, QLD, Australia, Jul. 2009, pp. 551–556.
[49] X. Hong, M. Gerla, G. Pei, and C.-C. Chiang, "A group mobility model for ad hoc wireless networks," in *ACM Int. Workshop Model., Anal. Simulation Wireless Mobile Syst.*, New York, NY, USA, 1999, pp. 53–60.
[50] J.-Y. Le Boudec and M. Vojnovic, "The random trip model: Stability, stationary regime, and perfect simulation," *IEEE/ACM Trans. Netw.*, vol. 14, no. 6, pp. 1153–1166, Dec. 2006.
[51] I. Rhee, M. Shin, S. Hong, K. Lee, S. J. Kim, and S. Chong, "On the Levy-walk nature of human mobility," *IEEE/ACM Trans. Netw.*, vol. 19, no. 3, pp. 630–643, Jun. 2011.
[52] D. Mitsche, G. Resta, and P. Santi, "The random waypoint mobility model with uniform node spatial distribution," *Wireless Netw.*, vol. 20, no. 5, pp. 1053–1066, Jul. 2014.
[53] J. B. Kuipers, *Quaternions and Rotation Sequences : A Primer with Applications to Orbits, Aerospace, and Virtual Reality*. Princeton, NJ, USA: Princeton Univ. Press, 1999.
[54] T. Milligan, "More applications of Euler rotation angles," *IEEE Antennas Propag. Mag.*, vol. 41, no. 4, pp. 78–83, Sep. 1999.
[55] C. Bettstetter, H. Hartenstein, and X. Pérez-Costa, "Stochastic properties of the random waypoint mobility model," *Wireless Netw.*, vol. 10, no. 5, pp. 555–567, Sep. 2004.
[56] R. R. Roy, *Random Waypoint Mobility*. Boston, MA, USA: Springer, 2011, pp. 65–124.
[57] F. R. K. Chung, J. A. Salehi, and V. K. Wei, "Optical orthogonal codes: Design, analysis and applications," *IEEE Trans. Inf. Theory*, vol. 35, no. 3, pp. 595–604, May 1989.
[58] J. A. Salehi, "Emerging optical CDMA techniques and applications," *Int. J. Opt. Photon.*, vol. 1, no. 1, Mar. 2007.
[59] D. C.-H. Chen, B. J. Sheu, and W. C. Young, "A CDMA communication detector with robust near-far resistance using paralleled array processors," *IEEE Trans. Circuits Syst. Video Technol.*, vol. 7, no. 4, pp. 654–662, Aug. 1997.
[60] J. A. Salehi and C. A. Brackett, "Code division multiple-access techniques in optical fiber networks. II. systems performance analysis," *IEEE Trans. Commun.*, vol. 37, no. 8, pp. 834–842, Aug. 1989.
[61] T. Ohtsuki, "Performance analysis of indoor infrared wireless systems using PPM CDMA," *Electron. Commun. Jpn. I, Commun.*, vol. 85, no. 1, pp. 1–10, Jan. 2002.
[62] S. Zahedi and J. A. Salehi, "Analytical comparison of various fiber-optic CDMA receiver structures," *J. Lightw. Technol.*, vol. 18, no. 12, pp. 1718–1727, Dec. 2000.
[63] F. Xu, M. Khalighi, and S. Bourennane, "Impact of different noise sources on the performance of PIN-and APD-based FSO receivers," in *Proc. Int. Conf. Telecommun. (ConTel)*, Graz, Austria, Jun. 2011, pp. 211–218.
[64] Behlouli, P. Combeau, S. Sahuguède, A. Julien-Vergonjanne, C. Le Bas, and L. Aveneau, "Impact of physical and geometrical parameters on visible light communication links," in *Proc. Adv. Wireless Opt. Commun. (RTUWO)*, Riga, Latvia, Nov. 2017, pp. 73–76.
[65] K. Lee, H. Park, and J. R. Barry, "Indoor channel characteristics for visible light communications," *IEEE Commun. Lett.*, vol. 15, no. 2, pp. 217–219, Feb. 2011.
[66] *SI PIN photodiodes: S5106, S5107, S7509, S7510*, HAMAMATSU Photon., Tokyo, Japan, May 2018.
[67] G. P. Agrawal, *Fiber-Optic Communications Systems*. Hoboken, NJ, USA: Wiley, 1992.
[68] S. Zahedi, J. A. Salehi, and M. Nasiri-Kenari, "M-ary infrared CDMA for indoors wireless communications," in *Proc. 12th IEEE Int. Symp. Pers., Indoor Mobile Radio Commun. (PIMRC)*, San Diego, CA, USA, vol. 2, Oct. 2001, pp. 6–10.
[69] J. B. Carruthers and P. Kannan, "Iterative site-based modeling for wireless infrared channels," *IEEE Trans. Antennas Propag.*, vol. 50, no. 5, pp. 759–765, May 2002.
[70] H. Schulze, "Frequency-domain simulation of the indoor wireless optical communication channel," *IEEE Trans. Commun.*, vol. 64, no. 6, pp. 2551–2562, Jun. 2016.

MD JAHID HASAN received the B.Sc. degree in electrical and electronic engineering from American International University-Bangladesh (AIUB), Dhaka, Bangladesh, in 2011, and the joint international M.Sc. degree in smart systems integration from Heriot-Watt-University, Edinburgh, U.K., in 2016. He is currently pursuing the Ph.D. degree with the École Centrale de Marseille, Marseille, France, funded by Marie Sklodowska-Curie Vision ITN.

From 2012 to 2014, he worked as an ASIC Design Engineer with Fastrack Anontex Limited, Dhaka, Bangladesh. He also served as a Lecturer with the Department of Electrical and Electronic Engineering, AIUB, from 2017 to 2018. Since 2018, he has been an early-stage Researcher with Vision ITN project hosted by Oledcomm SAS., Paris, France. His research interests include optical wireless communications, digital signal processing, and FPGA-based implementation. He was a recipient of the Erasmus Mundus scholarship during his M.Sc. program from the period of 2014 to 2016.

MOHAMMAD ALI KHALIGHI (Senior Member, IEEE) received the Ph.D. degree in telecommunications from the Institut National Polytechnique de Grenoble, Grenoble, France, in 2002. He is currently an Associate Professor with École Centrale Marseille, Marseille, France, and the Head of the Telecommunications and IoT Group, at Fresnel Institute Research Laboratory. He is also serving as the Project Coordinator for the H2020 ITN MSCA VisIoN project (Visible-light-based Interoperability and Networking) and the Action Chair for the COST Action CA19111 NEWFOCUS (European Network on Future Generation Optical Wireless Communication Technologies). He has coedited the book *Visible Light Communications: Theory and Applications* (CRC Press, 2017). His main research interests include signal processing for wireless communication systems with an emphasis on the physical-layer aspects of free-space, underwater, and indoor visible-light optical communications. He was the corecipient of the 2019 Best Survey Paper Award of the IEEE Communications Society. He is also serving as the Editor-at-Large for the IEEE TRANSACTIONS ON COMMUNICATIONS and the Lead-Guest-Editor for IEEE OPEN JOURNAL OF THE COMMUNICATIONS SOCIETY, Special Issue on Optical Wireless Communications. He has also served as an Associate Editor for the *IET Electronics Letters* as well as a Guest Co-Editor for the *Optik Journal* (Elsevier).

JORGE GARCÍA-MÁRQUEZ received the M.Sc. and Ph.D. degrees in optics from the Universidad de Guanajuato, Mexico, in 1995 and 1998, respectively, and the Habilitation degree in photonics from the Université de Versailles Saint-Quentin, France, in 2013. He was an Electronics Engineer with Universidad Iberoamericana-León, Mexico, in 1994. He was a Researcher with the Centro de Investigaciones en Optica from 1999 to 2013, the former National Institute of Metrology, Paris, until December 2014, then a Senior Researcher with Oledcomm, until 2019. He is currently a Project Leader with the Pôle Photonique-Energétique, Laboratoire National de Métrologie et d'Essais, Trappes, France. His past and current research cover length measurements, phase recovery, optical super-resolution, modulation of light with liquid crystals, geometrical optics, optical links antennae, optical wireless communications, and lidars. He has published 37 peer-review articles and has filed 13 patents.

BASTIEN BÉCHADERGUE received the degree in engineering from ISAE-Supaero, Toulouse, France, the M.S. degree in communication and signal processing from Imperial College London, London, U.K., in 2014, and the Ph.D. degree in signal and image processing from UVSQ, University Paris–Saclay, France, in 2017, for his work on visible light communication and range-finding for automotive applications. He is currently in charge of the research activities with Oledcomm, a company specialized in optical wireless communication product development. His current research interests thus include optical wireless communications and especially LiFi but also optical positioning.